BASIC RESEARCH

Accumulated Spinal Axial Biomechanical Loading Induces Degeneration in Intervertebral Disc of Mice Lumbar Spine

Yang-jun Lao, MD[1,2†], Tao-tao Xu, MD[1†], Hong-ting Jin, PhD[1], Hong-feng Ruan, PhD[1], Ji-tao Wang, MD[1], Li Zhou, MD[1], Ping-er Wang, MD[1], Jian Wang, PhD[2], Jun Ying, MD[1], Yuan-bin Zhang, MD[1], Cheng Luo, MD[1], Fang-da Fu, MD[1], Pei-jian Tong, MD[1,3], Lu-wei Xiao, PhD[1,3], Cheng-liang Wu, PhD[1]

[1]*Institute of Orthopaedics and Traumatology, Departments of* [2]*Orthopaedics, Tongde Hospital and* [3]*Orthopaedics, Affiliated Hospital of Zhejiang University of Traditional Chinese Medicine, Zhejiang, China*

Objective: To investigate the effect of accumulated spinal axial biomechanical loading on mice lumbar disc and the feasibility of applying this method to establish a mice intervertebral disc degeneration model using a custom-made hot plate cage. In previous studies, we observed that the motion pattern of mice was greatly similar to that of humans when they were standing and jumping on their lower limbs. There is little data to demonstrate whether or not accumulated spinal axial biomechanical loading could induce intervertebral disc degeneration *in vivo*.

Methods: Twenty-four 0-week-old mice were randomly divided into model 1-month and 3-month groups, and control 1-month and 3-month groups (n = 6 per group). The model groups was transferred into the custom-made hot plate cage three times per day for modeling. The control group was kept in a regular cage. The intervertebral disc samples of the L_3–L_5 were harvested for histologic, molecular, and immunohistochemical studies after modeling for 1 and 3 months.

Results: Accumulated spinal axial biomechanical loading affects the histologic, molecular, and immunohistochemical changes of mice L_3–L_5 intervertebral discs. Decreased height of disc and endplate, fissures of annulus fibrosus, and ossification of cartilage endplate were found in morphological studies. Immunohistochemical studies of the protein level showed a similar expression of type II collagen at 1 month, but a slightly decreased expression at 3 months, and an increased expression level of type X collagen and matrix metalloproteinase 13 (MMP13). Molecular studies showed that ColIIa1 and aggrecan mRNA expression levels were slightly increased at 1 month ($P > 0.05$), but then decreased slightly ($P > 0.05$). ColXa1, ADAMTS-5, and MMP-13 expression levels werer increased both at 1 and 3 months ($P < 0.05$). In addition, increased expression of Runx2 was observed.

Conclusion: Accumulated spinal axial loading provided by a custom-made hot plate accelerated mice lumbar disc and especially endplate degeneration. However, this method requires further development to establish a lumbar disc degeneration model.

Key words: Biomechanical loading; Degeneration; Endplate; Intervertebral disc; Lumbar; Model

Introduction

Bipedalism separates human beings and the other mammals, but leads to an accumulated axial loading of cervical and lumbar intervertebral discs (IVD)[1–3]. As a result, human beings frequently suffer from diseases related to IVD degeneration that cause low back pain and neck pain.[4,5] However, the mechanism of the occurrence and development of IVD degeneration has not been clarified, which contributes to the limited options for clinical treatment[6,7].

Accumulated spinal axial biomechanical loading is a risk factor for IVD degeneration[2,5,8]. Many of the patients who suffer from discogenic low back pain experience

Address for correspondence Cheng-liang Wu, PhD, Institute of Orthopaedics and Traumatology of Zhejiang Province, Binwen Road 548, Hangzhou, China 310053 Tel: 0061-571-86613684; Email: liuxianguiji@outlook.com

Disclosure: The authors have no conflicts of interest to declare.

†These two authors contributed equally to this work and are first co-authors.

Received 5 September 2016; accepted 27 March 2017

exposure to accumulated spinal axial loading through, for example, driving or repetitive motion patterns[8]. Taking this into account, we designed a preliminary research plan and observed that the motion pattern of mice is greatly similar to humans when they are standing or jumping on their lower limbs. We developed a hot plate cage with a base that could be heated up; mice would stand on the hot plate and jump continuously using their lower limbs, and, thus, the spinal axial biomechanical loading would be accumulated constantly. Using this hot plate cage, we also observed some degenerative signs of the lumbar IVD of mice.

The present study was designed to observe the effects of accumulated spinal axial biomechanical loading on mice lumbar IVD, to explore the mechanism of lumbar IVD degeneration, and to establish a mice lumbar IVD degeneration model. Establishing an animal model is key to exploring the mechanism of the initiation and development of IVD degeneration; today, there are many models established by needle puncturing, which lead to a non-endplate injure[9–12]. Endplates play an important role in the biomechanical and nutritional functions of IVD. Biomechanically, the endplate absorbs and shares axial loads during activities of daily living[13,14]. Nutritionally, the endplate is the primary pathway for transport between vertebral capillaries and cells within the disk nucleus[15,16]. Therefore, a model with non-endplate injury means the endplate remains healthy, the nutrition supply remains intact, and the degeneration of IVD would not be impacted and the model not responsible for injury[17]. With this in mind, we used 24 9-week-old mice for 1 or 3 months to investigate the effects of accumulated spinal axial biomechanical loading on lumbar IVD, and examined the histologic, molecular and immunohistochemical changes in mice lumbar IVD. Our results clearly showed that accumulated spinal axial biomechanical loading would induce degeneration in IVD of mice lumbar spine, especially in the endplate.

Material and Methods

Compliance with Ethical Standards

All the animal procedures were approved by the Ethical Committee of Zhejiang Chinese Medical University.

Custom-made Hot Plate Cage

We have applied for a patent for our custom-made hot plate cage (CN205515023U); further details can be found at "http://www.pss-system.gov.cn." The cage contains two parts, the shell (Fig. 1A) and the separator (Fig. 1B); the whole cage is shown in Fig. 1C. The shell is at the bottom and can be heated; the separator was designed to prevent the mice huddling.

Animals and Modeling

For the present study, 24 9-week-old C57BL/6J mice (Shanghai Laboratory Animal Center) were randomly divided into an accumulated spinal axial biomechanical loading group (model group) and a control group (n = 12 per group). The model group was transferred into a custom-made hot plate cage that was preheated to 50°C three times per day, and then moved back to their regular cage 15 min after the first mouse starting jumping. Mice in the custom-made hot plate cage would jump as a result of the high temperature of the base of the cage (Fig. 2). The control group did not have any intervention and remained in the regular cage. The IVD samples of the lumbar spine were harvested

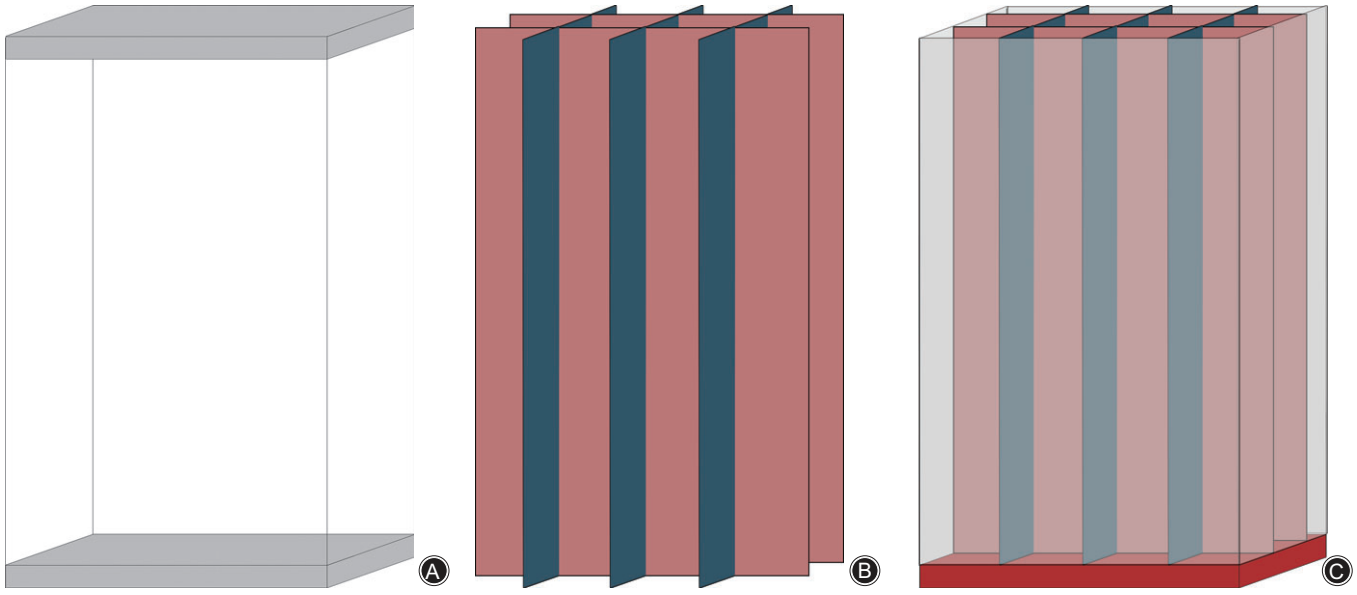

Fig. 1 The cage contained a shell with the bottom able to be heated up (A) and a separator (B) that prevented the mice from huddling. (C) The whole cage.

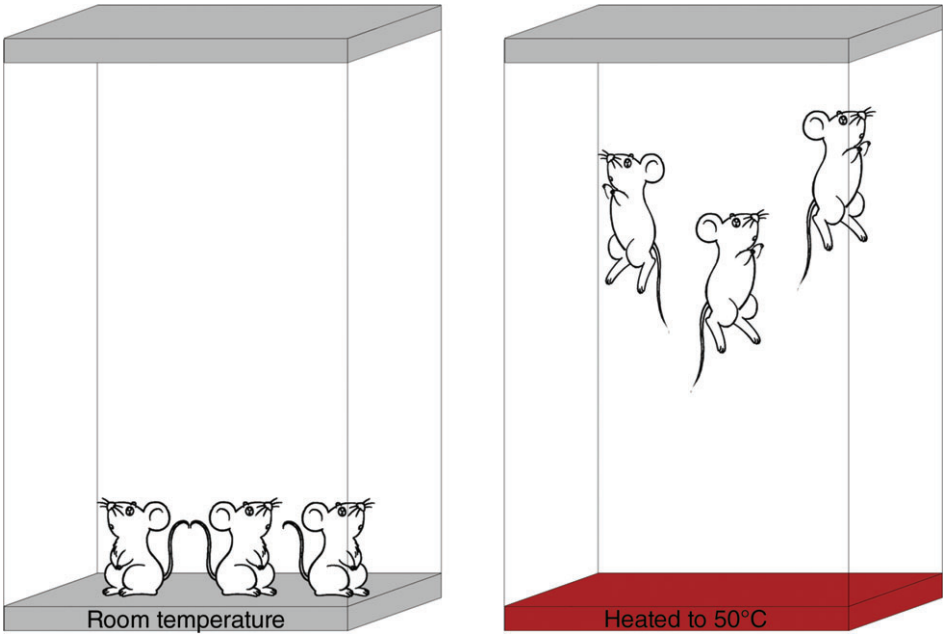

Fig. 2 Illustrative description of the custom-made hot plate cage, and the method of modeling. When mice were kept in a regular cage, the mice acted as usual; when in the cage heated to 50°C, the mice began to jump.

from L_3–L_5 for histologic, molecular, and immunohistochemical studies 1 and 3 months after modeling.

Histologic Evaluation

Mice from each group were killed 1 and 3 months after modeling. Then the lumbar spine samples from L_3–L_5 were harvested, fixed, decalcified with ethylenediaminetetraacetic acid, dehydrated by Tissue-Tek VIP5Jr (Sakura, Japan), cleared with dimethylbenzene, and then embedded in paraffin by EC 350-1 (Thermo, America). At least seven consecutive 3-μm sections were obtained from the coronal planes. Alcian Blue Hematoxylin/Orange G staining was given to both the model group and the control group simultaneously to examine the morphology of the annulus fibrous, nucleus pulposus and, cartilage endplate. The morphometric study was performed using the Image Analysis System (Olympus B × 50).

Immunostaining Study

Tissue sections were heated to 58°C overnight and then dewaxed, cleared, and rehydrated. The tissue sections were stained with collagen II (mab1330, Millipore), collagen X (A2884, biobyt), and matrix metalloproteinase 13 (MMP13, ab39012, Abcam) and antibody detection was performed using the Histostain-Plus Bulk Kit. The sections were digested with pepsin for 20 min, and then incubated in 3%H_2O_2 to block endogenous peroxidase activity for 10 min. Nonspecific binding sites were blocked by ready-to-use Reagent A. Then the sections were incubated with primary antibody at 4°C for 12 h. After a thorough wash, the sections were incubated with the ready-to-use Reagent B at room temperature for 10 min and then with ready-to-use Reagent C for 10 min. Following this, 3, 3-Diaminobenzidine (DAB) solution was used to elicit a color reaction. The sections were counterstained with hematoxylin and mounted. Specimens were examined by using an Image Analysis System (Olympus BX50).

Real-Time Polymerase Chain Reaction Analysis

Total RNA was isolated from L_3–L_5 IVD samples using an RNeasy Mini Kit (Qiagen, Hilden, Germany), cDNA was synthesized from 500 ng DNase-treated RNA through reverse transcription according to the PrimeScript RT Reagent Kit protocol (Takara Bio, Japan), Quantitative real-time PCR amplifications were performed using specific primers and an SYBR Green Real-time PCR kit. The primers used for the PCR are listed in Table 1 and the gel electrophoresis was done to make sure the primers were available. The thermal cycling conditions were as follows: an initial denature at 95°C for 3 min, followed by 40 cycles of 20 s of denaturing at 95°C, 20 s of annealing at 58°C, and 20 s of extension at 72°C. The levels of the target gene expression were normalized to that of β-actin in the same cDNA sample.

Statistical Analysis

All data are presented as the mean values ± standard deviation. The Student *t*-test was performed to compare lumbar disk height and thickness of the endplate between control and model groups at the same time point using SPSS software (SPSS10.0, Chicago, IL, USA); $P < 0.05$ was considered significant.

Results

Histopathological and Immunohistochemical Findings

Morphologic changes of the IVD between L_3–L_5 and adjacent endplate were checked by microscope, and well-organized annulus fibrosus, nucleus pulposus, and endplate

TABLE 1 Sequences of primers used in the real-time polymerase chain reaction

Genes	Forward primer	Reverse primer
Runx2 (234 bp)	5′-GTCCCAACTTCCTGTGCTCC-3′	5′-TCTTGCCTCGTCCGCTCC-3′
ColIIa1 (115 bp)	5′-ACTGGTAAGTGGGGCAAGAC-3′	5′-CCACACCAAATTCCTGTTCA-3′
MMP13 (173 bp)	5′-CTTCTTCTTGTTGAGCTGGACTC-3′	5′-CTGTGGAGGTCACTGTAGACT-3′
Adamts5 (110 bp)	5′-GGAGCGAGGCCATTTACAAC-3′	5′-CGTAGACAAGGTAGCCCACTTT-3′
ColXa1 (138 bp)	5′-CTTTGTGTGCCTTTCAATCG-3′	5′-GTGAGGTACAGCCTACCAGTTTT-3′
Aggrecan (150 bp)	5′-CCTGCTACTTCATCGACCCC-3′	5′-AGATGCTGTTGACTCGAACCT-3′
β-actin (241 bp)	5′-CACGATGGAGGGGCCGGACTCATC-3′	5′-TAAAGACCTCTATGCCAACACAGT-3′

were observed in the control group (Fig. 3A, B). After accumulated spinal axial loading modeling for 1 month, the lumbar disc structure became disorganized and small fissures were found in the outer layer of the annulus fibrosus (Fig. 3 C, D); larger fissures were found in the 3-month modeling samples (Fig. 4E, F). The cartilage endplate was gradually replaced by ossification. The alcian blue/orange G stain results of the extracellular matrix of modeling for 1 month were similar to the samples from the control group (Fig. 3C, D), while in samples of the 3 month modeling group, the stain of the extracellular matrix became thinner (Fig. 3E, F). Meanwhile, the height of the disk and endplate were measured. In the model groups, the height of disks (yellow arrows) was significantly decreased at 1 month and slightly decreased at 3 months when compared with the control group (1 month, $P = 0.007$; 3 month, $P > 0.05$, Fig. 3G), while the height of the endplate (red arrows) was decreased at all time points when compared with the control samples (1 month, $P = 0.022$; 3 month, $P = 0.001$; Fig. 3H).

Immunohistochemical study of the samples obtained from the accumulated spinal axial biomechanical loading group and the control group also revealed some differences.

Immunohistochemical study showed that when compared with the control group, the expression level of type II collagen was similarly after modeling in the 1 month group, but that decreased slightly 3 months after modeling. Moreover, the collagen X positive staining reached to the outer annulus fibrosus and the nucleus pulposus; both of 1 and 3-month modeling groups had stronger expression of collagen X compared with the control group, and it was much stronger in the 3 month group than in the 1 month group. In addition, the positive staining of MMP-13 of the 1 month and the 3 month group were found at the edge of the annulus fibrosus and nucleus pulposus, and was stronger in the 3 month group than in the 1 month group (Fig. 4).

Real-Time Polymerase Chain Reaction

Real-time PCR studies demonstrated that the mRNA expression level of two important components of extracellular matrix, colIIa1 and aggrecan, increased at 1 month while decreasing at 3 months; however, neither were significant ($P > 0.05$) compared with the sample obtained from control groups (Fig. 5A, C).

Meanwhile, the mRNA expression level of colXa1 also increased after modeling. In the control group, the expression level of colXa1 was similar for the 1 month and 3 month groups, while after modeling, the mRNA expression level of colXa1 increased significantly at both time points (1 month, $P = 0.000$; 3 month, $P = 0.000$; Fig. 5B).

The mRNA expression level of two important catabolic enzymes of extracellular matrix, ADAMTS-5 and MMP-13, increased at both of the two time points. In the control group, the expression of ADAMTS-5 and MMP-13 was gradually increased by aging. The expression of the three catabolic enzymes increased with the time of modeling. The accumulated spinal axial loading significantly increased MMP-13 (1 month, $P = 0.003$; 3 month, $P = 0.017$) and ADAMTS-5 (1 month, $P = 0.000$; 3 month, $P = 0.002$) mRNA expression at both time points compared with the control group (Fig. 5D, E).

Interestingly, the mRNA expression level of osteogenesis, Runx2, was also upregulated compared with the disk sample of the control group. It was increased significantly at 1 month after modeling ($P = 0.02$). The accumulated spinal axial loading increased the mRNA expression level of Runx2 slightly at 3 months ($P > 0.05$, Fig. 5F).

Discussion

Accumulated Spinal Axial Biomechanical Loading Induced Intervertebral Disc Degeneration

The objective of this study was to observe the effect of accumulated spinal axial biomechanical loading on mice lumbar IVD and to investigate the feasibility of applying this method to build a lumbar IVD degeneration model. The reason we chose this method was because the force pattern of mice lumbar IVD was similar to that for human beings when they were standing and jumping. The results of the present study provide direct evidence of morphologic changes in the IVD *in vivo*.

The reason we chose mice to check whether accumulated spinal axial biomechanical loading would induce mice lumbar IVD degeneration was because the average percent deviation of normalized disc geometry parameters of the mice lumbar was only 12%, which was the lowest compared with that of other animals[18]. The normalized torsional properties of mice were among the most similar to those of humans[19]. In addition, both the nurturing process and genotype of mice were normalized, so the individual difference could be controlled at a low level. Once a lumbar IVD

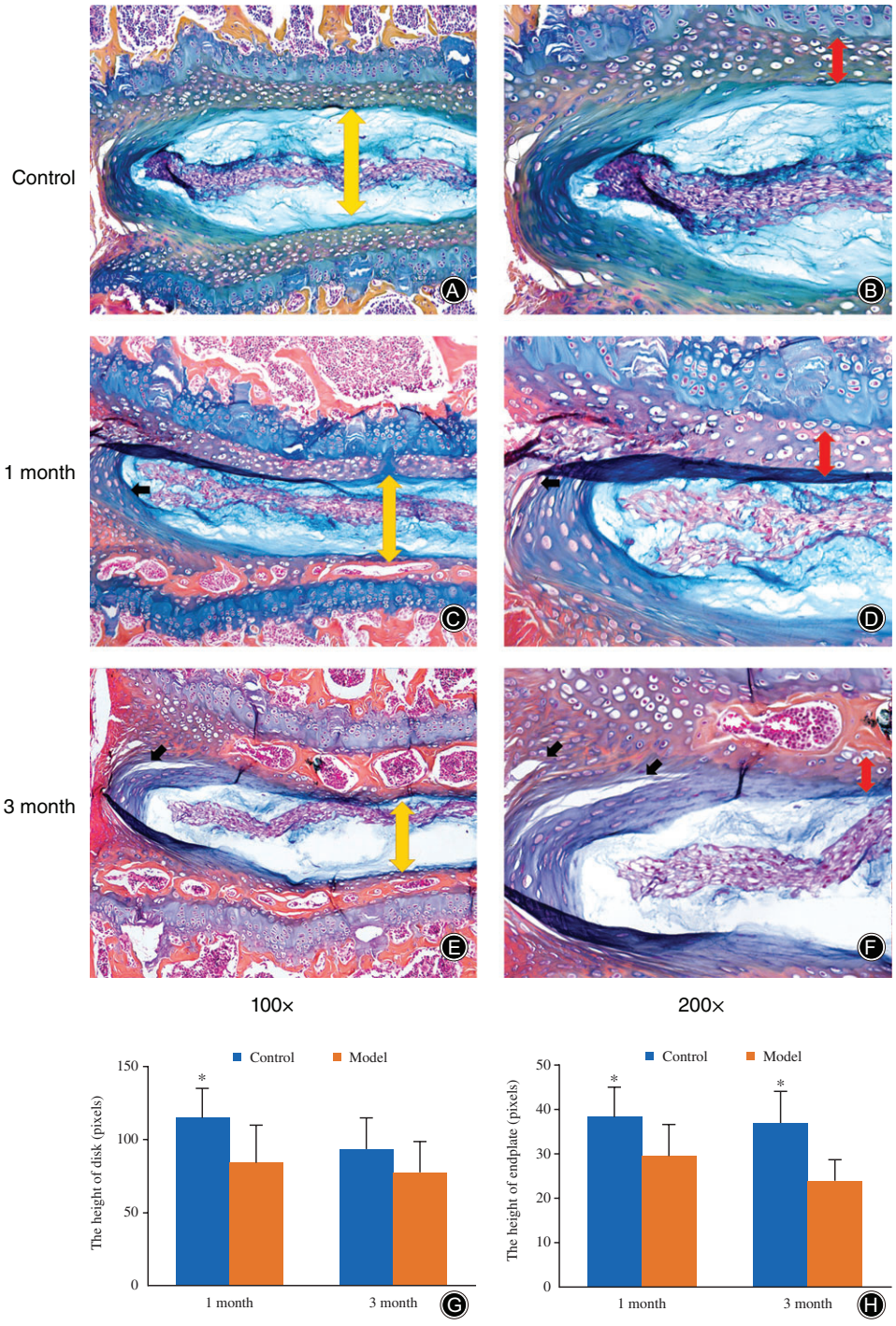

Fig. 3 Alcian blue/orange G staining of lumbar samples. In both of the model samples, the IVD structure became disorganized. In the model groups, the height of disks (yellow arrows) was significantly decreased at 1 month when compared with the control group (×100, A, C, G), while the height of the endplate (red arrows) was decreased at all time points when compared with the control samples (×200; B, D, H); fissures (black arrows) were found in the outer layer of the anulus fibrosus of the lumbar sample after modeling at both time points, but were larger at 3 months (E, F) compared to 1 month (B, D). The cartilage endplate was gradually replaced by ossification. The staining of the nucleus pulposus of the 3 month model group was thinner compared to that of the control group. More endplate ossification was developed in the 3-month group (E, F).

degeneration model is successfully established, a transgenic animal model could possibly be applied to investigate the mechanism.

As the results revealed, accumulated spinal axial biomechanical loading induced degenerative progress in mice lumbar IVD. First, we observed the morphologic changes in the model group and found that the height of both lumbar disk and cartilage endplate decreased after modeling; in the 3 month control group, the decrease of IVD may have resulted from the natural degeneration progress. Fissures in annulus fibrosus were observed in the model groups; the fissures became larger with the accumulation of biomechanical loading and time. The staining of the extracellular matrix also became thinner; for this, we infer that the synthesis and degradation balance of the extracellular matrix was broken by the accumulated biomechanical loading. The ossification

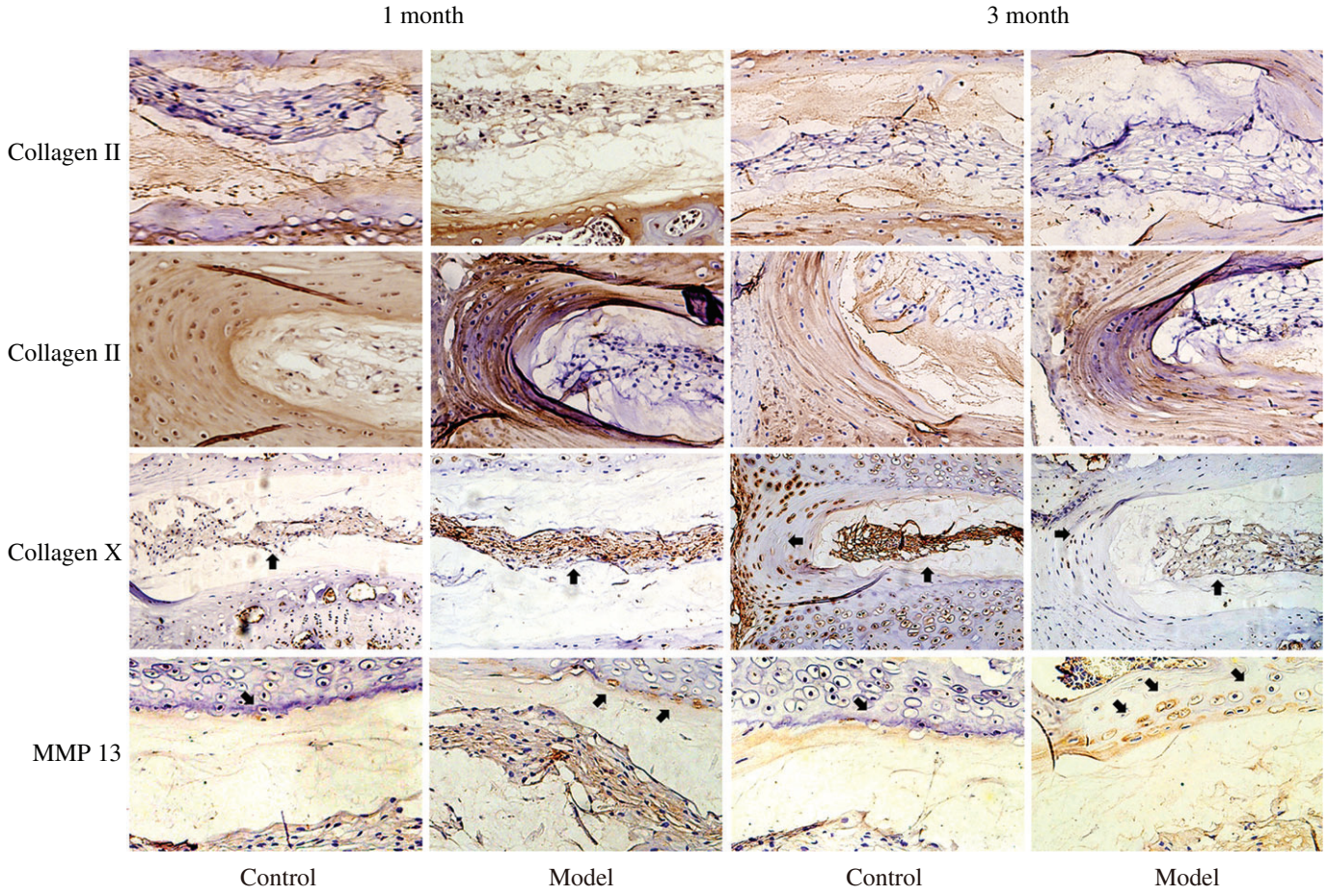

Fig. 4 Immunohistochemical assessments of the protein level of type II collagen, type X collagen, and MMP13. Immunohistochemical study showed that the protein level of type II collagen was decreased slightly after modeling in both 1 month and 3 month groups compared with the control group. The collagen X positive staining reached to the outer annulus fibrosus and the nucleus pulposus, and that of the 3-month group was stronger than for the 1-month group. The positive staining of MMP-13 of the 1-month and 3-month groups reached to the edge of the annulus fibrosus and nucleus pulposus, and was stronger for the 3-month group than for the 1-month group.

of the cartilage endplate accelerated with time. Immunohistochemical and PCR results also support the morphologic study. After 1 month modeling, although the expression of catabolic enzymes of the extracellular matrix increased, with the balance of anabolic and catabolic still existing, the two important components of extracellular matrix increased compensatively. With the accumulation of biomechanical loading, however, once the metabolic balance of the extracellular matrix was disturbed, the level of collagen II and aggrecan decreased.

Limitations

At first, the aim of this study was to establish a new lumbar IVD degeneration model of mice, because the animal model is key to exploring the mechanism of initiation and development of IVD degeneration. An appropriate animal model needs to simulate not only the geometry and torsional properties, but the predisposition accumulated daily. Today, there are so many ways to establish an IVD degeneration model, such as mechanical loading, needle puncture and transgenic methods, with the most widely used method being needle puncture[9–11]. The IVD degeneration model established here involves no endplate injury, so that the endplate remains healthy, which may be the very key to recovery of the IVD; in other words, the needle-puncture IVD degeneration model is responsible for trauma-caused IVD degeneration[20] rather than degeneration caused by accumulated axial biomechanical loading.

Conclusion

In conclusion, accumulated axial biomechanical loading induced degenerative changes in the lumbar IVD of mice. Using the custom-made hot plate cages, we found that the force pattern of accumulated biomechanical loading was similar to that of humans. The morphological changes, including the decreased height of IVD and cartilage endplate, were

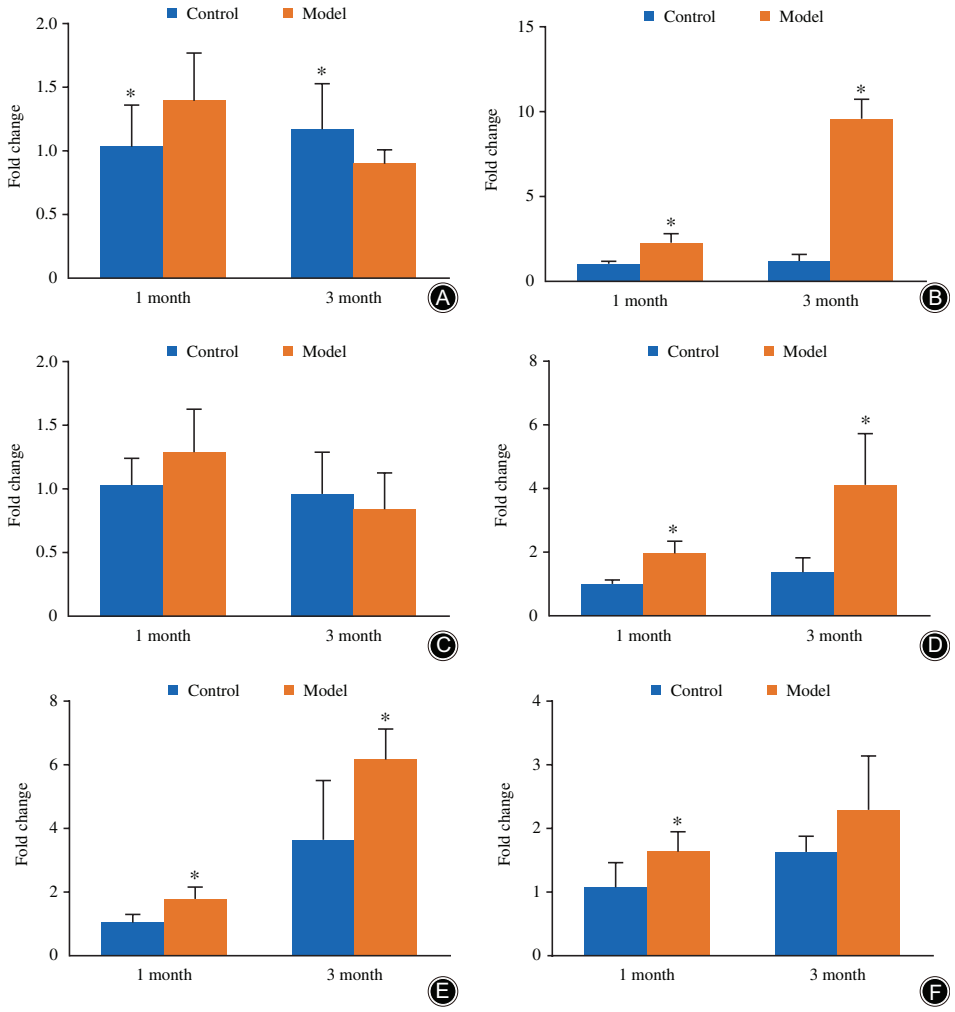

Fig. 5 The mRNA expression of ColIIa1, aggrecan, ColXa1, MMP-13, ADAMTS-5, and Runx2. In the model group, the mRNA expression of ColIIa1 and aggrecan decreased but not significantly (A, C), while that of ColXa1, MMP-13, and ADAMTS-5 were significantly upregulated (B, D, E), and that of Runx2 also had the trend of upregulating compared with the control group at the same time after modeling (F). The columns represent the mean ± standard deviation of six independent experiments.

similar to clinical appearance. Although the model was obviously different from the human situation, the accumulated biomechanical loading lumbar IVD degeneration model may expand our knowledge regarding the occurrence and development of IVD degeneration, and also may help explain why osteophytes and spinal stenosis occur.

Acknowledgments

The present study was supported by the National Natural Science Foundation (81273770), the National Natural Science Foundation (81373669), and the Zhejiang Provincial Natural Science Foundation of China (LZ12H270001 and LY15H270012).

References

1. Walter BA, Korecki CL, Purmessur D, Roughley PJ, Michalek AJ, Iatridis JC. Complex loading affects intervertebral disc mechanics and biology. Osteoarthritis Cartilage, 2011, 19: 1011–1018.
2. Walsh AJ, Lotz JC. Biological response of the intervertebral disc to dynamic loading. J Biomech, 2004, 37: 329–337.
3. Hsieh AH, Lotz JC. Prolonged spinal loading induces matrix metalloproteinase-2 activation in intervertebral discs. Spine (Phila Pa 1976), 2003, 28: 1781–1788.
4. Le Maitre CL, Binch AL, Thorpe A, Hughes SP. Degeneration of the intervertebral disc with new approaches for treating low back pain. J Neurosurg Sci, 2015, 59: 47–61.
5. Kimura S, Steinbach GC, Watenpaugh DE, Hargens AR. Lumbar spine disc height and curvature responses to an axial load generated by a compression device compatible with magnetic resonance imaging. Spine (Phila Pa 1976), 2001, 26: 2596–2600.
6. Mannion AF, Brox JI, Fairbank JC. Comparison of spinal fusion and nonoperative treatment in patients with chronic low back pain: long-term follow-up of three randomized controlled trials. Spine J, 2013, 13: 1438–1448.
7. Siepe CJ, Heider F, Wiechert K, Hitzl W, Ishak B, Mayer MH. Mid- to long-term results of total lumbar disc replacement: a prospective analysis with 5- to 10-year follow-up. Spine J, 2014, 14: 1417–1431.
8. Lewis C, Johnson P. Whole-body vibration exposure in metropolitan bus drivers. Occup Med (Lond), 2012, 62: 519–524.
9. Barczewska M, Wojtkiewicz J, Habich A, *et al*. MR monitoring of minimally invasive delivery of mesenchymal stem cells into the porcine intervertebral disc. PLoS One, 2013, 8: e74658.
10. Jones P, Gardner L, Menage J, Williams GT, Roberts S. Intervertebral disc cells as competent phagocytes in vitro: implications for cell death in disc degeneration. Arthritis Res Ther, 2008, 10: R86.
11. Anderson DG, Markova D, An HS, *et al*. Human umbilical cord blood-derived mesenchymal stem cells in the cultured rabbit intervertebral disc: a novel cell source for disc repair. Am J Phys Med Rehabil, 2013, 92: 420–429.
12. Tam V, Rogers I, Chan D, Leung VY, Cheung KM. A comparison of intravenous and intradiscal delivery of multipotential stem cells on the healing of injured intervertebral disk. J Orthop Res, 2014, 32: 819–825.

13. Arjmand N, Plamondon A, Shirazi-Adl A, Parnianpour M, Larivière C. Predictive equations for lumbar spine loads in load-dependent asymmetric one- and two-handed lifting activities. Clin Biomech (Bristol, Avon), 2012, 27: 537–544.
14. Quinnell R, Stockdale H, Willis D. Observations of pressures within normal discs in the lumbar spine. Spine (Phila Pa 1976), 1983, 8: 166–169.
15. Lotz JC, Fields AJ, Liebenberg EC. The role of the vertebral end plate in low back pain. Global Spine J, 2013, 3: 153–164.
16. Roberts S, Menage J, Urban J. Biochemical and structural properties of the cartilage end-plate and its relation to the intervertebral disc. Spine (Phila Pa 1976), 1989, 14: 166–174.
17. Alini M, Eisenstein SM, Ito K, *et al*. Are animal models useful for studying human disc disorders/degeneration?. Eur Spine J, 2008, 17: 2–19.
18. O'Connell GD, Vresilovic EJ, Elliott DM. Comparison of animals used in disc research to human lumbar disc geometry. Spine (Phila Pa 1976), 2007, 32: 328–333.
19. Showalter BL, Beckstein JC, Martin JT, *et al*. Comparison of animal discs used in disc research to human lumbar disc: torsion mechanics and collagen content. Spine (Phila Pa 1976), 2012, 37: E900–E907.
20. Sakai D, Andersson GB. Stem cell therapy for intervertebral disc regeneration: obstacles and solutions. Nat Rev Rheumatol, 2015, 11: 243–256.